Proceedings of the 21st ICSMGE, Vienna, Austria, 14 – 19 June 2026. Pistrol, Adam & Schweiger (eds.)
Published by: ÖGG, Austrian Society for Geomechanics, Salzburg, Austria, ISBN 978-3-9503898-4-5
https://doi.org/10.53243/ICSMGE2026-2175

Seismic Performance Evaluation of a Zoned Earth Dam through Field-Calibrated Numerical Analysis

Camilo Marulanda, William Ruíz
INGETEC, Bogotá, Colombia, marulanda@ingetec.com.co; wruiz@ingetec.com.co

Juan-Pablo Castillo Betancourt, Jaime Azuaje
INGETEC, Bogotá, Colombia, jpablocastillo@ingetec.com.co; azuajejaime@gmail.com

ABSTRACT: Adequate evaluation of earthquake-induced deformations in earth dams is key to ensuring their stability and safe operation. Numerical models calculate the seismic response in the time domain, for which the resulting deformations largely depend on the stiffness module adopted to represent the soil behavior. This paper presents the case of a 90 m high zoned earth fill dam mainly composed of sandy silt with filters on top of a rigid foundation. The constitutive model used for the dams was HS Small. Initial stiffness was calibrated through the combined use of shear wave velocity (Vs) measurements and settlement data obtained from geotechnical instrumentation present at the construction stage. The model was implemented using Plaxis to perform coupled dynamic calculations to predict the deformations induced by a group of earthquake events selected for the analysis. Values for E_{50}, E_{oed}, and E_{ur} deformation modulus were selected based on the approaches proposed by Wichtmann (2017), Alpan (1970), and Benz & Vermeer (2007). Also, the adjustment coefficients of these expressions were calibrated for each dam material using back-analysis adjusting the settlements measured during construction. Several models were prepared using the calibrated parameters, and varying moduli values to assess result sensitivity to stiffness. Obtained deformation values can be used to evaluate the dam's safety conditions and freeboard loss.

KEYWORDS: Dam, seismic analysis, response, calibration, border conditions, dynamic.

1 INTRODUCTION

The seismic performance of large earth structures such as embankment dams is of critical importance, particularly in regions of moderate and high seismicity. This study presents the dynamic analysis of a 90-meter-high embankment dam constructed during the 1980's with slopes 2.5H:1V upstream and 2.0H:1V downstream, including buttress berms, constructed primarily with sandy silt and underlain by a rigid foundation. The dam's geometry and material zoning are presented in Figure 1.

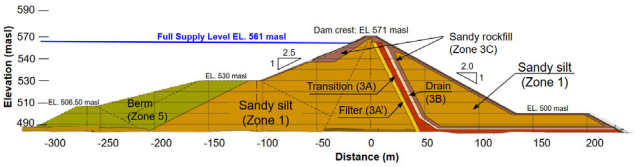

Figure 1. Cross section of the dam and its zonation.

Characterization of the dam materials was done based on data from original construction documentation, as well as the results from several new seismic velocity measurements. The Hardening Soil model with small-strain stiffness (HS-Small) was chosen for use in the dynamic analyses. This model captures the nonlinear stiffness degradation behavior and the damping response that is critical for simulating cyclic loading conditions in fine-grained soils. The model can also account for stiffness increase with confining pressure, thus providing a more adequate spatial distribution of material properties than simpler models such as Linear Elastic or Mohr-Coulomb. Only the dam foundation bedrock was characterized with a linear elastic model.

For an adequate initial stress state, the model incorporated a simplified version of the staged construction process of the dam, thus allowing calculation of realistic initial stress conditions. The water table at the interior of the dam was determined with steady state flow analysis. Next, the boundary conditions required for dynamic analysis were applied to the model; this enabled to avoid wave reflection in the side and bottom of the model, and to account for the effect of the reservoir. For the study of the dynamic response, a set of four (4) motions was used, considered representative of a zone with intermediate seismicity. The chosen seismic records received basic signal treatment for use in the dynamic calculations, including baseline correction and slight low pass filtering.

Finite element calculations in Plaxis were used, using coupled flow analysis to account for pore pressure excess accumulation during seismic shaking, allowing a more realistic evaluation of the dam's response under earthquake loading. Separate evaluations of post-earthquake stability were done for limit equilibrium.

For the dynamic calculation, the result analysis centered on maximum and final displacements, excess pore pressure development, acceleration responses, and stability under seismic loading, offering valuable insights into the dam's performance under strong ground motion scenarios as well as for the analysis of similar structures.

2 MATERIAL PROPERTIES

The dam is primarily composed of sandy silt, with drain and filter zones along the upstream and slope, placed over a rock foundation. A berm composed of loosely compacted construction residues, originally placed as a disposal site, now contributes to stabilizing the upstream slope of the dam.

Figure 2 shows the gradation bands for the different zones that make up the dam fills, where it can be observed that the main fill (Zone 1) consists of a silty sand, resulting from the blasting of siltstone, sandstone, and conglomeratic sandstone strata available in the project area.

For the numeric model, the rigid foundation layer was modeled as linear elastic with an elastic moduli of 1 GPa, given its high stiffness relative to the embankment materials and its minimal expected contribution to overall deformation during seismic loading. The Hardening Soil model with small-strain stiffness (HS-Small) was adopted for the embankment and filter materials due to its ability to capture nonlinear stiffness

degradation and recover small-strain behavior—crucial under seismic loading. This model also accounts for confining pressure dependency and stress-path sensitivity, which are especially relevant for cyclic and dynamic loading conditions.

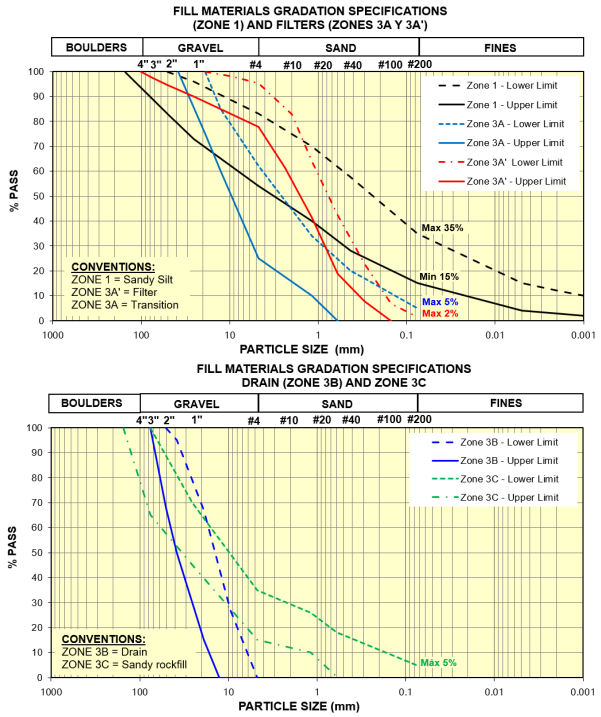

Figure 2. Particle size distribution bands for dam fill materials.

The material stiffness parameters for these models were derived from the settlements measured during construction, and in-situ seismic velocity measurements (see Figure 3), ensuring consistency between static and dynamic stiffness assumptions.

The measured seismic velocities are of 350 m/s +/- 70 m/s at the surface, and increase to 600 m/s at a 30 m depth. Thus, a range of 275 – 800 MPa of the initial shear stiffness is derived from the field measurements.

These results were used to calibrate the HS Small model based on the expressions by Wichtmann (2017), Alpan (1970), and Benz & Vermeer (2007). The most relevant expressions used are presented now, starting with the max shear modulus:

$$G_{max} = A_{G_d} \frac{\left(a_{G_d} - e\right)^2}{1+e} \left(\frac{p}{p_{atm}}\right)^{nG_d} \quad (1)$$

Where e is the void ratio, p the mean stress, p_{atm} the reference pressure of 100 kPa, and the other three (A_{G_d}, a_{G_d} and nG_d) are a series of values for the parameters was suggested based on the different materials tested, and for this study the values were calibrated.

For the stiffness at large strain, the corresponding expression was:

$$E_{50} = A_{E_s} \frac{\left(a_{E_S} - e_{50}\right)^2}{1+e_{50}} \left(\frac{p_{50}}{p_{atm}}\right)^{nE_S} p_{atm} \quad (2)$$

Which is a function of the void ratio and mean pressure at the corresponding level of strain, and the parameters A_{E_s} and a_{E_S} were also calibrated.

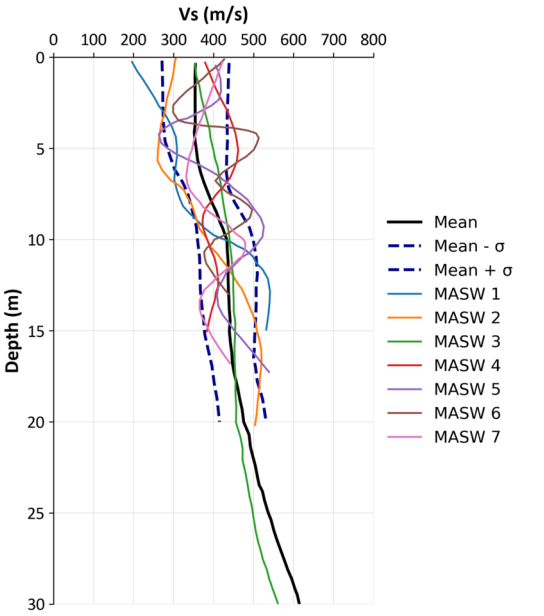

Figure 3. Seismic velocity measurements of the dam and its immediate surroundings.

As part of this study, these correlations were rewritten as:

$$E_{oed}/_{E_0} = \theta * \rho^{\alpha} * V_s^{\beta} \quad (3)$$

where ρ is the density in kN/m^3, and Vs is the shear wave velocity in m/s. The values used for the coefficients α, β, and θ are summarized in Table 1.

Table 1. Adjustment coefficients for equation 3

Material	α	β	θ
Sandy silt	0.85	1.67	5e-7
Drain/filter	0.85	1.75	4e-7
Berm	0.85	1.67	5e-7

Material strength parameters such as the friction angle, cohesion, and dilatancy angle were calibrated using data from construction records and post-construction monitoring of settlements and deformations.

Figure 4 displays the displacement contours after simulated staged construction is completed, showing up to 35 cm of settlement towards the middle of the dam. These contours result from varying the material moduli to reproduce the 35-40 cm value recorded at the end of construction, as presented in Figure 5. Table 2 summarizes the key parameters used in dynamic analyses.

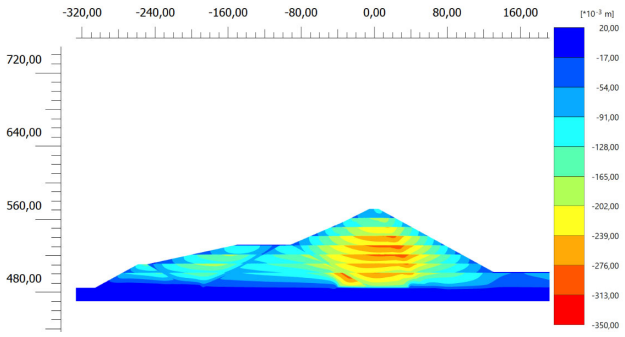

Figure 4. Vertical displacements of 35 cm after construction.

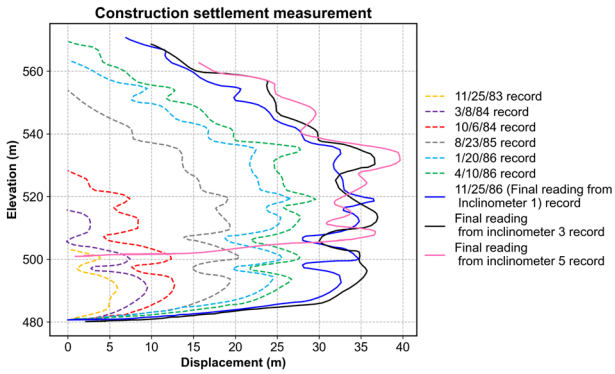

Figure 5. Variation of settlement with depth along the dam axis during construction.

Table 2. Material parameters for dynamic calculation

Parameter	Sandy Silt	Sandy Rockfill	Berm
Unit weight γ (kN/m³)	22	22	20
Cohesion c' (kPa)	3	2	2
Friction angle ϕ (°)	38	39	28
Stiffness modulus $E_{50_r}^{ef}$ (MPa)	85	63	45
Oedometer modulus $E_{oed_r}^{ef}$ (MPa)	76	54	36
Unloading reloading stiffness E_{urr}^{ef} (MPa)	240	170	135
Stiffness exponent *m*	0.64	0.52	0.60
Max shear moduli $G_{0_r}^{ef}$ (MPa)	235	210	163
Shear Strain $\gamma_{0.7}$	$0.137x10^{-3}$	$0.107x10^{-3}$	$0.146x10^{-3}$
Unloading/reloading Poisson ration ν (–)	0.30	0.20	0.30
Reference pressure P_{ref} (kPa)	100	100	100

3 METHODOLOGY

3.1 *Static Stability Assessment*

To evaluate static stability under operational conditions, a two-dimensional limit equilibrium analysis was performed using the Morgenstern-Price (1965) method, which allows for variable interslice force magnitudes and directions, while satisfying both force and moment equilibrium. This makes it a robust option compared to simpler methods, as it avoids assuming a fixed inclination of interslice forces. Stability was evaluated for three different reservoir levels: maximum, normal, and minimum operating levels. The dam geometry and material strengths were taken from the finite element model, and phreatic surfaces were adjusted accordingly.

3.2 *Dynamic Finite Element Modeling*

Dynamic response was evaluated using a fully coupled hydro-mechanical analysis in Plaxis, which accounts for pore pressure accumulation during seismic loading. Initial pore pressure distribution was assigned from a previous steady state flow calculation. The dam was modeled in 2D plane strain, with a staged construction procedure used to replicate realistic stress conditions prior to dynamic shaking.

The seismic input was applied as a prescribed base displacement at the model's compliant base, while free-field boundaries were used along the vertical sides to minimize wave reflection. Hydrodynamic effects of the reservoir were included using added mass elements (Westergaard, 1933; Zangar, 1953), representing the effective mass of water interacting with the upstream face during shaking. The dynamic calculations used the HSSmall model to capture stiffness degradation, and excess pore pressures were computed via the coupled formulation.

A set of 4 ground motions covering a wide range of frequency was used in the analysis. The response spectra at 5% damping for these motions is presented in Figure 6. The Pear Blossom ground motion has the highest peak at low periods, while the Parkfield motion carries content over the wider period range (0 to 0.6 seconds). The motions were recovered from the NGA West2 PEER database (Ancheta et al., 2014, PEER, 2024).

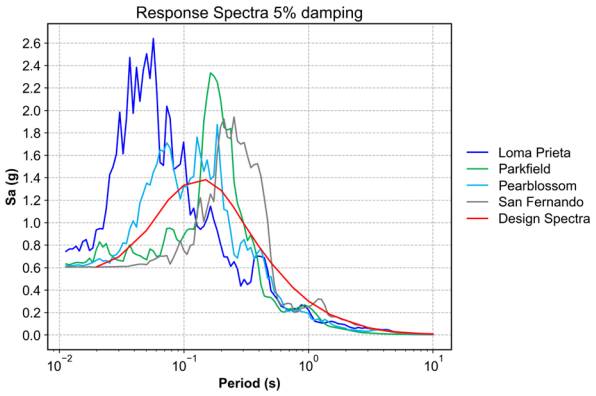

Figure 6. Response spectra for the motions corresponding to the signals used during dynamic analysis.

A heavily refined mesh comprising 30000 elements was used, to guarantee a small enough size of the elements for proper wave propagation (Vermmer & Verruijt, 1981).

4 RESULTS

4.1 *Slope Stability Analysis by Limit Equilibrium*

Figure 7 presents results of limit equilibrium analysis for the downstream side of the dam, while Figure 8 presents results for the upstream slope. The lowest computed safety factor corresponds to maximum reservoir level on the downstream side, where downstream slopes showed the least stability due to the influence of seepage and reduced confining stress. However, all computed factors of safety remained above 1.5, satisfying typical design criteria. The Morgenstern-Price method (1965) provided a reasonable failure mechanism, with critical slip surfaces developing above the downstream berm.

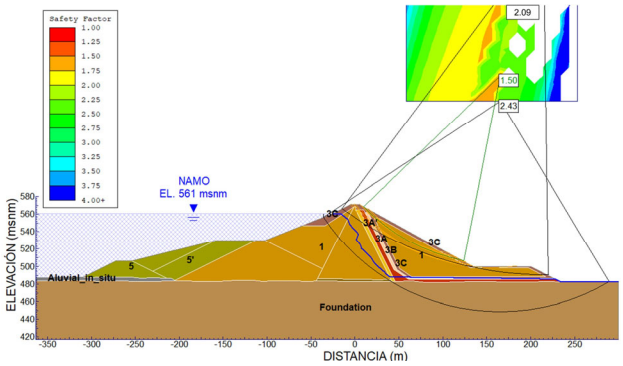

Figure 7. Results for downstream stability of the dam under static conditions.

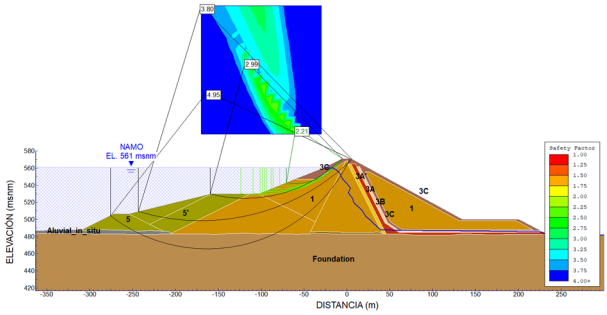

Figure 8. Results for upstream stability of the dam under static conditions.

Sensitivity analysis was performed to assess the effect of the reservoir, and the results are presented in Figure 9. It can be seen that while the effect on downstream stability is limited, a variation of 0.2 in the safety factor can occur as a result of varying the reservoir level. A complementary sensitivity analysis on the compacted zones confirmed that, as expected given the high level of compaction, the resulting factors of safety were high.

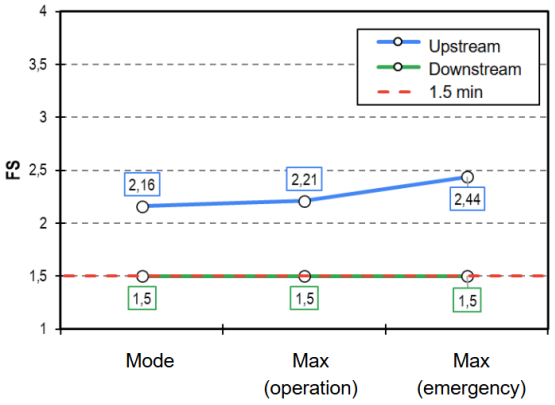

Figure 9. Minimum stability factors for different reservoir levels.

Next, the pseudo-static stability response was evaluated using a similar limit equilibrium analysis. These calculations included both horizontal and vertical seismic components to study the response under extremely unfavorable conditions. As seen in Figure 10 and Figure 11, these extreme conditions result in FS values lower than one. While we recognize the inherent limitations of the pseudo-static method, it was adopted as an initial screening tool for this stage of the assessment.

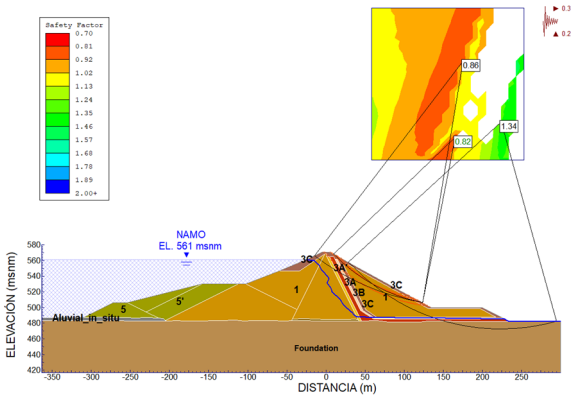

Figure 10. Results for downstream stability of the dam under pseudo-static conditions.

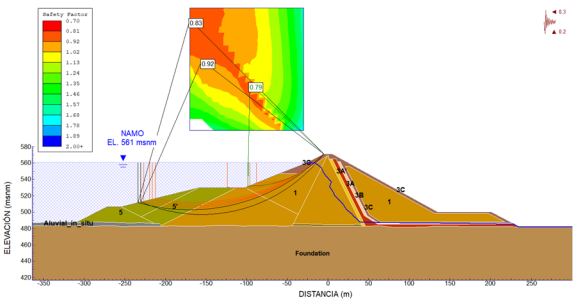

Figure 11. Results for upstream stability of the dam under pseudo-static conditions.

4.2 *Dynamic Response*

Figure 12 shows the acceleration time history recorded at the rock foundation (grey) and the top of the crest of the model (red), where an amplified acceleration value at the crest appears through most of the motion.

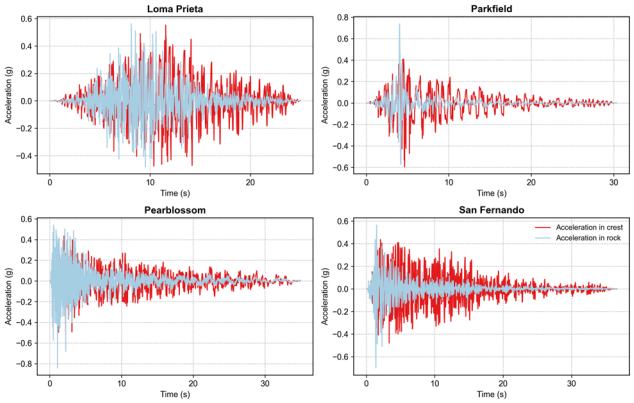

Figure 12. Acceleration time history showing motion amplification.

The dynamic analyses revealed moderate crest displacements and significant excess pore pressure accumulation, particularly within the core zone and near interfaces with filter materials. Figure 13 shows vertical displacement contours after shaking for one representative input motion. Settlements with a maximum value of 35 cm occur along the crest after the seismic motion, with the highest values located at the crest.

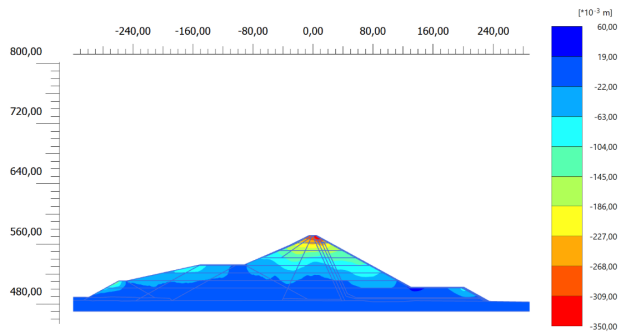

Figure 13. Settlement contours after dynamic analysis with the Parkfield motion.

Peak horizontal displacements at the crest ranged from 16 to 30 cm, depending on the input motion characteristics. However, the highest value of horizontal displacements occur not at the crest but at the bottom of the slopes of the dam, with maximum displacements in each direction at the foot of the upstream and downstream slopes of the dam, as can be seen in Figure 14.

Maximum displacement on the upstream slope is as high as 52 cm, while the downstream displacements can reach 32 cm; these highest values occur towards the middle of the slopes.

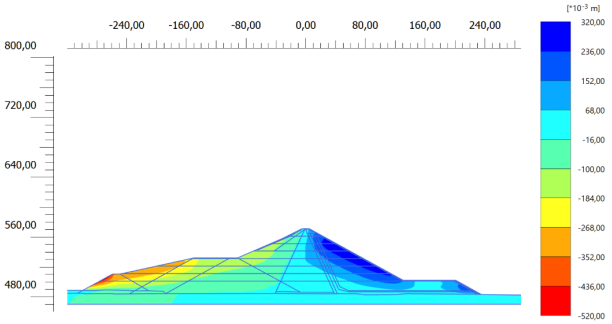

Figure 14. Horizontal displacement contours after seismic analysis with the Parkfield motion.

The evolution of these displacements was recorded at the locations of these maximum values. The record of settlement is presented in Figure 15, which shows the highest value results from the Parkfield motion (the one for which the contours were presented).

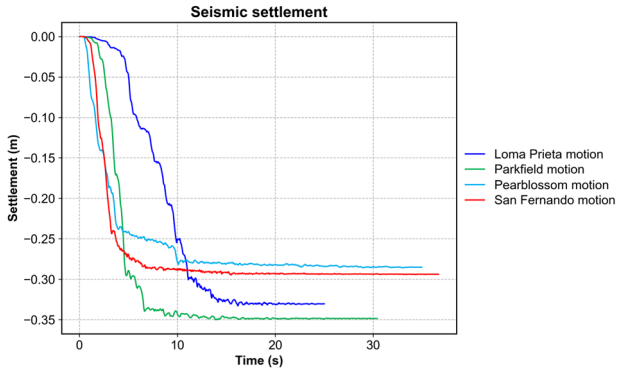

Figure 15. Settlement time histories for the computed motions.

The time histories corresponding to the location of maximum displacement in the downstream slope are presented in Figure 16, while those for the location of maximum upstream displacement are shown in Figure 17. Again, the highest values for the final displacements correspond to the Parkfield motion. However, higher values can be seen during the motion, and even the maximum displacement in the downstream slope occurs at 14 seconds for the Loma Prieta motion.

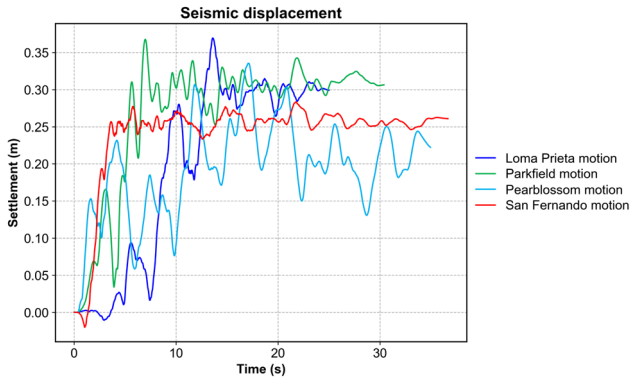

Figure 16. Horizontal displacement time histories for the computed motions, downstream slope

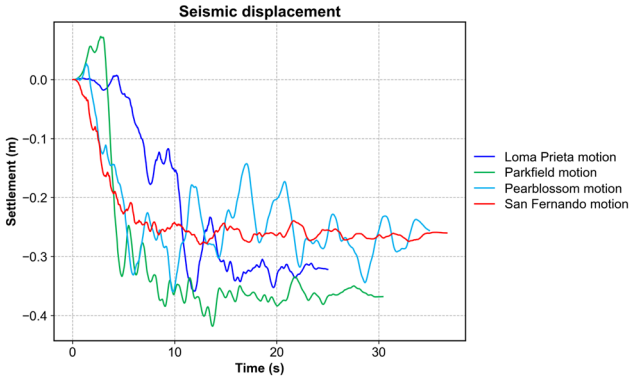

Figure 17. Horizontal displacement time histories for the computed motions.

To observe wave propagation, a column of nodes was placed along the dam axis every 20 m to recover response spectra. These results are presented in Figure 18 for the Parkfield motion a) and the Loma Prieta motion b), the ones inducing the higher displacements. This figure show how the wave initially de-amplifies as it traverses the fills of the dam until the last 40 m, where it amplifies heavily first in the range of 0.2<T<0.8 s, and then over the whole 0.1<T<0.9 s range. Maximum amplification occurs at values of T of 0.15 and 0.45 s.

a)

b)

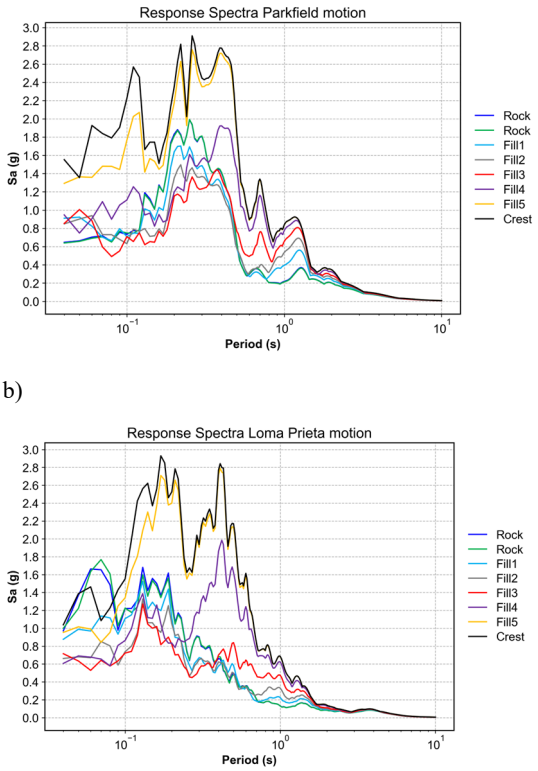

Figure 18. Response spectra showing wave propagation for the a) Parfkield motion and the b) Loma Prieta motion.

The response to the cycling loading of the different motions is portrayed in Figure 19, where shear strain values reach up to 0.004 under the Loma Prieta motion and 0.003 with the Parkfield motion. The accumulation of important shear strain after numerous cycles is apparent, as well as the effect of the numerous cycles involved in each chosen seismic signal. The Loma Prieta and Parkfield motions exert similar shear stresses

as high as 60-80 kPa on the dam fills, and result in the higher shear strains and displacements.

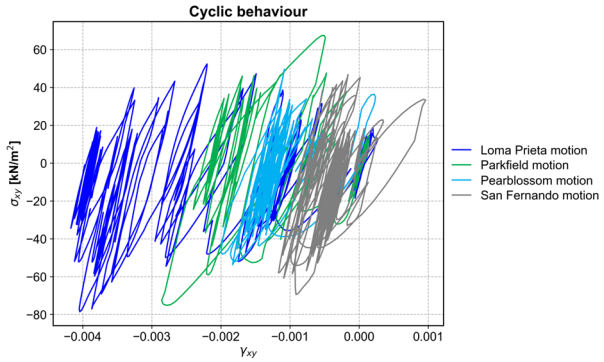

Figure 19. Response of the dam fills under cyclic loading.

5 CONCLUSIONS

The dynamic numerical analysis conducted in this study provides comprehensive insights into the behavior of the earth dam under seismic loading conditions. By integrating field-measured data, including shear wave velocity profiles and in-situ construction monitoring, the analysis achieves a realistic simulation of the dam's response, capturing key parameters such as settlement, horizontal displacement, and response spectra through different soil layers.

5.1 *Stability Analysis and Implications for Dam Safety*

The stability analysis conducted under dynamic loading conditions demonstrates a significant reduction in factors of safety (FoS) during peak seismic excitation. The minimum dynamic FoS recorded was of 0.86 for the downstream slope and of 0.83 for the upstream slope, compared to a static FoS of 1.5 and 2.21 respectively. It must be kept in mind that these results are under extremely unfavorable conditions including a very high vertical component. These are even lower than one, thus indicating the expected occurrence of high displacements under seismic response.

Importantly, the spatial distribution of shear strain and displacements after the seismic calculation, suggests that certain zones—especially near the crest and the bottom end of the slopes—are more susceptible to strength degradation.

5.2 *Settlement and Horizontal Displacement Time Histories*

The settlement time histories reveal a progressive accumulation of vertical deformation throughout the seismic event. The motions with the higher frequency content in the range of 0.1<T<1s reach this maximum value already at 5 seconds, while the other motion, with more content in the range of 0.01<T<0.1s takes about 10 s to do so. As expected, the highest settlement values occur near the top of the dam.

Horizontal displacement time histories similarly demonstrate peak ground response predominantly at the upper part of both the upstream and downstream slopes. However, maximum values occur not at the top of the embankments but in the case of the upstream slope towards the lowest part of the berm as can be seen in Figure 14. The figure also shows that however, most of the face of the upstream slope has smaller values than the downstream face of the dam. These results show a non-trivial behavior observed in the model that would be less likely to occur if a hydrostatic condition was used to model the reservoir instead of the hydrodynamic one used for this model.

5.3 *Wave propagation*

This stratified response emphasizes the importance of detailed site characterization in dynamic analyses. The varying spectral characteristics across layers have direct implications for the stability and deformation mechanisms of the dam, as the collected response spectra across the dam showed, with different instances of amplification and de-amplification that can exceed factors of 2 as seen in the ranges of 0.1<T<0.2s and of 0.4<T<0.6s in Figure 18. For example, the amplified response in the intermediate fill layers likely contributes to localized strain accumulation, potentially triggering shear failure zones if seismic intensities exceed the design threshold.

5.4 *Model Validation and Limitations*

The methodology of combining in-situ measurements with numerical modeling serves as a valuable template for similar earth dam projects, enabling more robust seismic hazard assessments and risk mitigation strategies. Continued refinement of this approach, including real-time data assimilation and probabilistic modeling, could further enhance dam safety management. Installation of proper instrumentation, including topographic controls and accelerometer equipment can provide valuable information for such calibrations when recording response to actual seismic events.

Moreover, the reliance on shear wave velocity as a proxy for dynamic stiffness and damping properties introduces some uncertainty, particularly in heterogeneous or anisotropic soil layers where velocity variations can be significant. Future work should consider integrating additional geophysical methods or advanced soil testing (e.g., cyclic triaxial tests) to refine these parameters.

Finally, the estimated seismic-induced deformations indicate that the dam is expected to experience settlements and lateral displacements within the freeboard allowance. Consequently, the vulnerability of the dam under the design validation earthquake is considered acceptable.

6 REFERENCES

Alpan, I. (1970). The empirical evaluation of the deformation modulus of soils. Soils and Foundations, 10(3), 59–65. https://doi.org/10.3208/sandf1960.10.3_59

Ancheta, T.D., Darragh, R.B., Stewart, J.P., Seyhan, E., Silva, W.J., Chiou, B.S.-J., Wooddell, K.E., Graves, R.W., Kottke, A.R., Boore, D.M., Kishida, T., and Donahue, J.L. (2014). NGA-West2 Database.

Benz, T., & Vermeer, P. A. (2007). A hypoplastic model for unsaturated soils with stress-dependent strength. International Journal for Numerical and Analytical Methods in Geomechanics, 31(3), 251–274. https://doi.org/10.1002/nag.591

Morgenstern, N.R., and Price, V.E. 1965. The analysis of the stability of general slip surfaces. Géotechnique, 15(1): 79-93.

PEER Ground Motion Database. (Accessed on 31/07/2024). Pacific Earthquake Engineering Research Center, University of California, Berkeley. https://ngawest2.berkeley.edu

Vermeer, P.A., Verruijt, A. (1981). An accuracy condition for consolidation by finite elements. Int. J. for Num.

Anal. Met. in Geom., 5, 1-14.

Westergaard, H. M. (1933). "Water pressures on dams during earthquakes." Trans. ASCE 98 (2): 418–432.

Wichtmann, T. (2017). Strain accumulation and pore pressure generation in sand due to cyclic loading: Experiments and constitutive modelling. Habilitation thesis, Ruhr-Universität Bochum.

Zangar C. N. (1953). "Hydrodynamic Pressures on Dams Due to Horizontal Earthquake Effects," Engineering Monograph, No. 11, Bureau of Reclamation.